Geofísica Internacional (1991), Vol. 30, Num. 1, pp. 43-54

Stress drops for foreshocks and aftershocks of the 1979 Petatlán, Mexico, earthquake

D. A Novelo-Casanova
Instituto de Geofísica, Universidad Nacional Autónoma de México

Received: October 24, 1990, accepted: April 11, 1991.

RESUMEN
Las caídas de esfuerzos de premonitores y réplicas ($3.5 \leq M_L \leq 4.0$) del temblor de Petatlán ($M_s = 7.6$) ocurrido en México en 1979, fueron examinadas con el propósito de obtener un mejor conocimiento de las propiedades mecánicas del material y del proceso de ruptura existente en una zona de subducción bastante joven. Los esfuerzos fueron calculados estimándose la dimensión de la fuente a partir de la anchura del medio ciclo de la onda P y del momento sísmico obtenido a partir de una fórmula empírica apropiada para la región. Los resultados indican una distribución irregular de esfuerzos en toda el área de réplicas y proporcionan evidencias que apoyan un modelo de dos asperidades en la fuente.

PALABRAS CLAVE: Caída de esfuerzos, premonitores, réplicas, temblor de Petatlán.

ABSTRACT
Stress drops for foreshocks and aftershocks ($3.5 \leq M_L \leq 4.0$) of the 1979 Petatlán, Mexico, earthquake ($M_s = 7.6$) were examined with the purpose of understanding the mechanical properties of rock and the failure process of a very young subduction zone. The static stress drop was calculated by estimating the source dimension from the width of the P-wave half-cycle and the seismic moment from a moment-magnitude relation appropriate to the region. Values of stress drop indicate an irregular distribution throughout the aftershock zone and support a two-asperity model in the source area.

KEY WORDS: Stress drops, foreshocks, aftershocks, Petatlán earthquake.

INTRODUCTION

Stress drop is one of the parameters which determines the level of acceleration produced by an earthquake. Regional variations in stress drop may have importance in seismic risk analysis.

Static stress drop is the difference between the initial (tectonic loading) stress and the static frictional stress (Brune, 1970). Static stress-drop estimates for large and great earthquakes range from 10 to 100 bars. Simple techniques exist for estimating this parameter from body wave data for small and moderate-sized earthquakes (Boatwright, 1980). Stress drops of small earthquakes may be calculated from short-period seismograms, even when they are clipped (Frankel and Kanamori, 1983; O'Neill, 1984).

Foreshocks and aftershocks of the 1979 Petatlán, Mexico, earthquake ($M_s = 7.6$) were recorded on analog magnetic tape by the Hawaii Institute of Geophysics during the Rivera Ocean Seismic Experiment (Ewing and Meyer, 1982). The seismic network distribution, the main shock epicenter location and the aftershock area are shown in Figure 1. Station parameters and recording and processing of data were reported by Gettrust *et al.* (1981) and Hsu *et al.* (1983). In this study we analyze the two-week period of foreshocks immediately preceding and the four-week period of aftershocks immediately following the main shock. All events are located within a one-degree square from 17°N to 18°N and 101°W to 102°W.

The study showed that the stress drops were irregularly distributed throughout the Petatlán aftershock area and that the spatial stress drop distribution supports a two-asperity model proposed by Novelo-Casanova *et al.* (1984) and Hsu *et al.* (1985).

METHOD OF ANALYSIS

We use the method of Frankel and Kanamori (1983) to compute the rupture duration and the stress drop of earthquakes between magnitudes 3.5 and 4.0. The time between the P-wave onset and the first zero crossing is measured directly from the seismogram ($\zeta_{1/2}$) to estimate the rupture duration. Then $\zeta_{1/2}$ is corrected for the effects of path and instrument using the waveform of small foreshocks and aftershocks ($1.8 \leq M_L \leq 2.8$) as empirical Green's functions. We did not considered events with magnitude greater than 4.0 because their pulse widths may represent several subevents.

The source time duration (ζ_{source}) as defined by the P-wave is found by subtracting (in effect deconvolving) the minimum pulse width (ζ_{min}) from the pulse width of the shock ($\zeta_{1/2}$) to be analyzed. The pulse width is taken as the time between the P-wave onset and the first zero crossing on the seismogram. The minimum pulse width is determined from small events close to the analyzed event. The small event waveform is assumed to be the impulse response of the path between the source and receiver, convolved with the instrument response. Since the waveforms

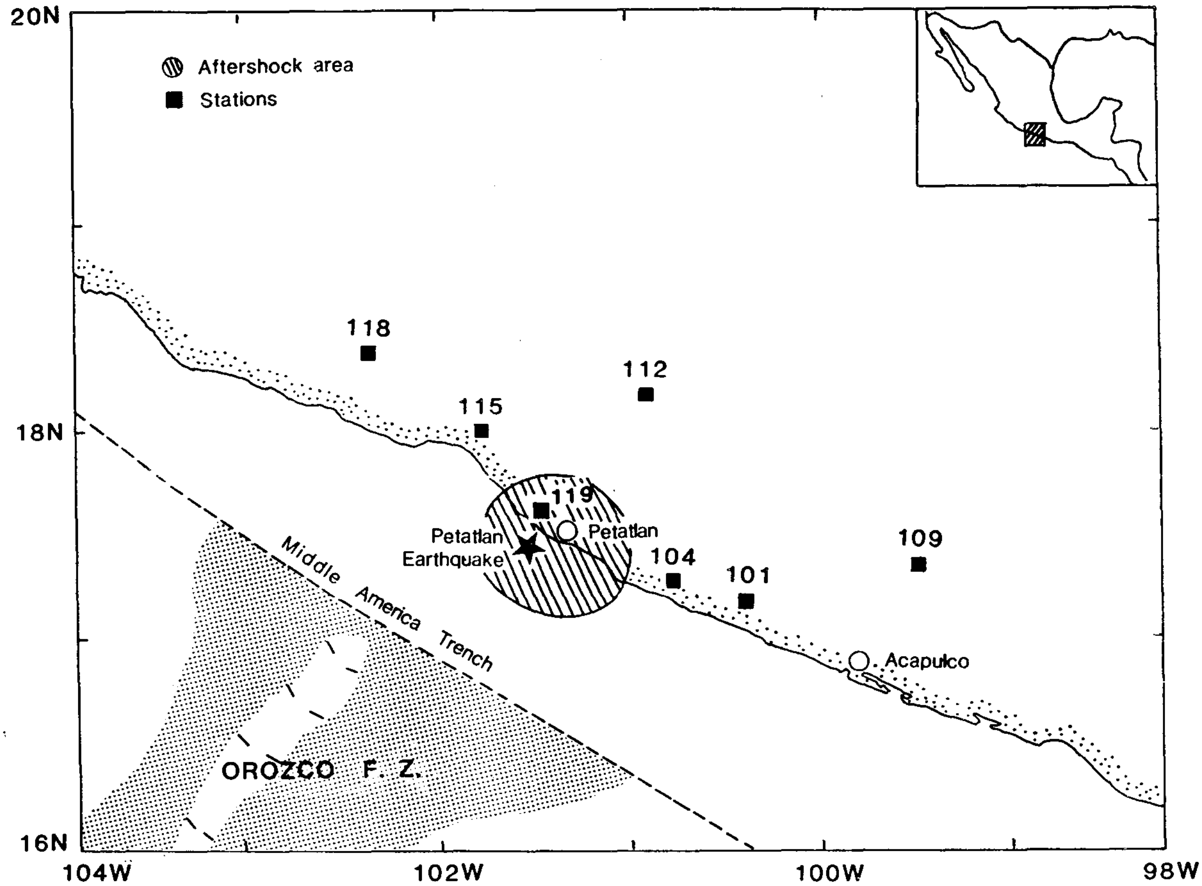

Fig. 1. Hawaii Institute of Geophysics temporary stations that recorded the Petatlán earthquake and its aftershocks. As in Fig. 4, the aftershock area is defined by events that ocurred during the first 54 hr immediately following the mainshock (Novelo-Casanova *et al.*, 1984).

of the event to be analyzed and the minimum pulse-width event are recorded by the same instrument, "deconvolving" one waveform from the other effectively corrects for the instrument response and the path on ζ_{source}. However, the source duration can only be determined when the rupture times are sufficiently long to be separated from the pulse broadening caused by the path.

The fault radius (r) for a circular rupture is given by (Boatwright, 1980):

$$r = \frac{\zeta_{source}\, v}{1-(v/c)\sin\theta} = \frac{(\zeta_{1/2}-\zeta_{min})\, v}{1-(v/c)\sin\theta} \qquad (1)$$

where c = P-wave velocity, v = rupture velocity, θ = angle between the normal to the fault plane and the outgoing seismic ray.

A rupture velocity of 3.75 km/s is assumed. The P-wave velocity is taken to be 6.5 km/s and θ is assumed equal to 45° for all calculations. These values are adopted as average values.

The seismic moment M_o was calculated empirically from the local magnitude M_L:

$$\log_{10} M_o = 17.33 + 1.05\, M_L\,, \qquad (2)$$

a relation derived by Meyer *et al.* (written communication, 1983) from P spectra of Petatlán aftershocks.

M_L was determined from coda duration. It may not be directly related to M_o. The purpose of this work, however, is to obtain relative and not absolute values of stress drops σ. The exact form of the empirical moment-magnitude relation is not crucial to the results of this paper because we are studying events in a limited magnitude range.

Once the fault radius r and seismic moment M_o are determined, σ is determined from Brune's (1970) formula for a circular fault:

$$\sigma = (7/16)\, M_o/r^3 \qquad (3)$$

Stress drop measurements obtained from pulse widths may not be comparable in their absolute values to those obtained from the corner frequency of the displacement spectra. Our purpose, however, is to detect relative differences in rupture duration and static stress drop.

The pulse widths were measured directly from the seismograms of stations 104, 112 and 115 (Figure 1), recorded from two weeks prior to four weeks after the mainshock. Data from station 119, which began recording two weeks after the mainshock, were also used.

Sampling rates for analog-to-digital conversion were 50 samples/s for stations 104 and 112, and 38 samples/s for stations 115 and 119. However, pulse widths were estimated to an accuracy of 0.005 sec by linear interpolation.

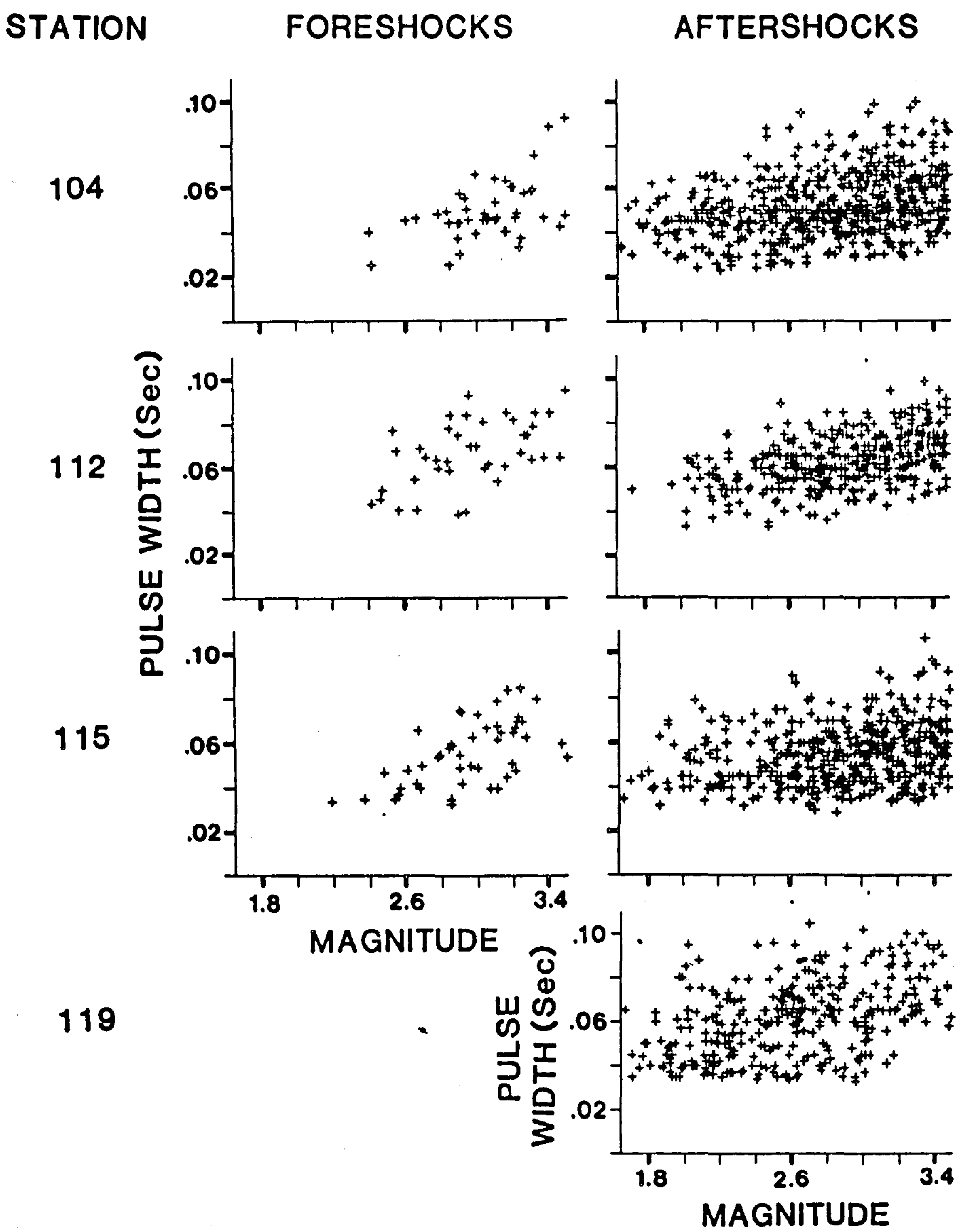

Fig. 2. Pulse width versus magnitude. Note the near-constant minimum width for earthquakes below about magnitude 2.7.

Figure 2 shows the measured pulse widths versus magnitude for different stations. From these plots we computed the mean lower bound of the pulse width for each station (Table 1). This average minimum width ζmin was used to compute the fault radius (equation 1). We used only one ζmin per station since the region is strongly heterogeneous.

Average source parameters were computed only for events with impulsive first P-wave arrival and reliable pulse width observed at two or more stations. Epicentral (ERH) and depth (ERZ) errors ≤ 5.0 km, and Root Mean Square (RMS) error of travel time residuals ≤ 0.5 s were also required.

Stress drops were determined for events of magnitude $M_L \leq 3.2$ (foreshocks) and ≤ 3.5 (aftershocks). These thresholds were chosen so that rupture times would be sufficiently long to be separated from the pulse broadening caused by the path and the instrument response. A total of 9 foreshocks and 57 aftershocks met this selection criterion.

For each event the average stress drop <SD> was calculated after Archuleta *et al.* (1982):

$$<SD> = 10^{(1/N) \sum_{i=1}^{N} \log_{10} SD_i} \tag{4}$$

where N is the number of stations for which stress drops were computed and SD_i is the stress drop at the ith station. The standard deviation (s.d.) of the log (stress-drop) is given by:

$$s.d.(\log_{10} <SD>) = \left\{ \frac{1}{N-1} \sum_{i=1}^{N} (\log_{10} SD_i - \log_{10} <SD>)^2 \right\}^{1/2} \tag{5}$$

The multiplicative error (ESD) is:

$$ESD = 10^{\{s.d(\log_{10} <SD>)\}} \tag{6}$$

Thus, when <SD> is plotted on a logarithmic scale, the standard deviation will be ESD.

This procedure gives equal weight to all stress drop observations. If one were to average stress drops arithmetically these averages would be biased toward the larger values.

RESULTS

Figure 2 shows the measured pulse widths as a function of magnitude for events of magnitude less than 3.5. The pulse widths scatter above a minimum value that remains approximately constant with magnitude.

Table 1 shows the arithmetic average minimum pulse width (ζ_{min}) adopted for each station. These averages were obtained from the lower bounds of events with M ≤ 2.7 displayed in Figure 2. Δ* is the approximate distance between the center of the aftershock area and the stations.

Table 1

Minimum pulse width values

Station	Average ζ_{min} (sec)	Δ* (km)
Foreshocks		
104	.025	72
115	.034	82
112	.040	98
Aftershocks		
119	.037	30
104	.028	72
115	.034	82
112	.037	98

* measured from the center of the aftershock area to the seismic station.

Table 2 lists the earthquake parameters for the foreshocks and aftershocks for which the stress drop was calculated. The estimated source parameters for these events are presented in Table 3. The pulse widths of Table 1 were used to correct for the effect of the path and the instrument on the initial pulse of the earthquakes. Only one foreshock and seven aftershocks in Table 3 had error factors (ESD) greater than 2.0 (i.e., more than 100% error as referred to the average value).

Figure 3 displays the aftershock stress-drop versus magnitude for events with ESD ≤ 1.45. Not simple correlation between these two parameters is evident. Thus, the calculated stress drops do not show an evident dependence on moment within this limited range of magnitude.

DISCUSSION

Computation of source dimensions from the pulse width presents a major difficulty due to: (a) the variability of the pulse widths (Table 3) for a given event; (b) incomplete azimuthal coverage to constrain the rupture geometry; and (c) uncertainties in the minimum pulse width measurements. The initial pulse width on the seismogram is a function of the rupture duration, the instrumental response, and the broadening caused by the apparent attenuation of the path. If the observed average minimum pulse width is much larger than the true minimum, the source radius will

Table 2

Events for which stress drops were computed

Event No.	Origin Time YrMoDa HrMn		Latitude (N)	Longitude (W)	Depth (km)	Mag.	RMS@ (s)	ERH* (km)	ERZ* (km)
Foreshocks									
1	790303	2230	17.262	101.248	3.52	3.27	0.45	3.4	2.6
2	790304	331	17.859	101.546	33.37	3.63	0.28	2.6	2.3
3	790304	448	17.322	101.313	2.64	3.21	0.43	2.8	2.3
4	790304	20 9	17.349	101.209	10.84	3.31	0.26	1.9	1.6
5	790308	842	17.262	101.327	1.55	3.20	0.34	2.7	2.4
6	790308	927	17.396	101.280	11.60	4.03	0.32	4.6	3.1
7	790309	17 4	17.398	101.222	8.89	3.38	0.33	1.9	1.8
8	790310	1833	17.490	101.488	6.98	3.41	0.25	4.2	3.9
9	790312	1550	17.515	101.423	13.78	3.33	0.33	3.6	2.0
Aftershocks									
1	790314	12 6	17.840	101.136	11.42	3.90	0.26	3.3	3.4
2	790314	13 5	17.628	101.518	20.50	4.30	0.02	1.7	0.4
3	790314	1318	17.404	101.533	12.74	3.62	0.19	4.1	3.5
4	790314	1348	17.252	101.529	13.92	4.02	0.11	4.0	2.3
5	790314	1423	17.426	101.562	9.86	3.67	0.42	2.8	2.8
6	790314	1436	17.461	101.472	13.49	3.50	0.34	2.4	2.3
7	790314	1443	17.486	101.591	15.18	3.56	0.18	2.1	2.6
8	790314	1450	17.434	101.616	13.91	3.57	0.28	2.5	2.3
9	790314	1512	17.438	101.474	11.45	3.53	0.40	4.7	3.7
10	790314	1525	17.318	101.457	9.17	4.18	0.14	3.4	2.5
11	790314	1729	17.731	101.525	22.19	3.52	0.45	4.2	4.6
12	790314	1815	17.419	101.406	7.27	3.87	0.31	3.3	1.7
13	790314	1837	17.387	101.560	16.11	3.60	0.27	2.2	1.6
14	790314	1856	17.474	101.378	5.12	3.91	0.35	4.4	4.5
15	790314	1936	17.344	101.596	10.72	3.67	0.29	3.7	2.9
16	790314	2032	17.378	101.549	9.39	3.53	0.32	4.1	2.5
17	790314	2034	17.348	101.216	13.89	4.02	0.23	3.8	2.2
18	790314	2223	17.385	101.600	8.90	3.73	0.34	3.8	2.4
19	790314	2234	17.273	101.418	1.12	3.71	0.49	5.0	2.7
20	790314	2236	17.334	101.554	7.08	3.50	0.49	3.4	3.3
21	790314	23 9	17.475	101.530	13.14	3.52	0.40	2.9	3.0
22	790315	013	17.391	101.558	9.74	3.75	0.07	1.5	1.0
23	790315	123	17.428	101.634	4.49	3.72	0.29	3.0	3.5
24	790315	2 1	17.456	101.624	15.99	3.80	0.37	4.9	3.1
25	790315	3 6	17.349	101.549	8.93	3.50	0.37	2.4	2.0
26	790315	639	17.225	101.227	19.67	3.81	0.47	3.7	3.1

Table 2 (continued)

Events for which stress drops were computed

Event No	Origin YrMoDa	Time HrMn	Latitude (N)	Longitude (W)	Depth (km)	Mag.	RMS[@] (s)	ERH[*] (km)	ERZ[*] (km)
27	790315	8 1	17.408	101.501	9.03	3.80	0.18	2.0	1.1
28	790315	848	17.459	101.545	12.30	3.54	0.30	2.2	2.5
29	790315	1018	17.439	101.472	12.70	3.69	0.29	2.1	1.9
30	790315	1037	17.332	101.524	24.82	3.68	0.43	4.0	4.2
31	790315	1120	17.386	101.526	12.10	3.58	0.30	2.6	2.5
32	790315	1212	17.380	101.572	11.78	3.71	0.29	2.5	3.0
33	790315	1330	17.406	101.513	24.99	3.54	0.40	4.2	5.0
34	790315	1449	17.339	101.637	17.69	3.67	0.41	3.4	3.7
35	790315	1512	17.278	101.280	7.01	3.77	0.49	3.2	2.5
36	790315	1723	17.351	101.221	11.42	4.01	0.22	4.0	3.3
37	790315	1745	17.391	101.626	18.73	3.76	0.50	4.1	3.5
38	790315	1750	17.519	101.312	17.27	3.68	0.40	3.1	2.9
39	790315	2154	17.407	101.567	12.05	3.75	0.25	2.0	1.9
40	790316	248	17.304	101.569	10.35	3.66	0.37	3.1	3.3
41	790316	3 6	17.303	101.582	12.50	3.93	0.25	2.4	2.5
42	790316	335	17.300	101.299	8.97	3.59	0.50	3.4	3.7
43	790316	338	17.529	101.493	22.64	3.95	0.50	4.3	3.7
44	790316	646	17.241	101.309	4.60	3.59	0.48	3.1	2.7
45	790316	655	17.280	101.262	20.18	3.88	0.42	3.6	3.4
46	790316	737	17.499	101.246	8.80	3.56	0.48	2.9	3.1
47	790316	924	17.418	101.494	9.34	3.50	0.34	2.2	2.2
48	790316	1010	17.418	101.318	18.75	4.14	0.08	0.9	1.2
49	790316	1140	17.418	101.540	9.04	3.58	0.48	3.1	2.7
50	790316	1324	17.372	101.366	0.81	3. 8	0.23	2.9	1.5
51	790316	1954	17.581	101.193	0.79	3.63	0.25	4.6	3.4
52	790323	234	17.432	101.355	2.74	3.64	0.23	3.8	3.1
53	790324	034	17.462	101.636	5.06	3.64	0.17	2.5	3.3
54	790325	4 6	17.116	101.622	19.20	4.05	0.50	4.4	3.9
55	790327	2124	17.506	101.264	23.49	3.53	0.42	3.4	2.4
56	790330	1345	17.588	101.210	13.40	3.95	0.26	3.2	4.1
57	790407	1242	17.543	101.268	3.45	3.60	0.36	0.6	0.3

@ Root mean error of time residuals.
* Standard error, ERH = epicenter location error; ERZ = focal depth error.

Table 3

Source parameters@ of earthquakes listed in Table 2

Event No.*	Moment (10^{21} dyne-cm)	Station 104 $\zeta_{1/2}$	Station 104 SD	Station 112 $\zeta_{1/2}$	Station 112 SD	Station 115 $\zeta_{1/2}$	Station 115 SD	Station 119 $\zeta_{1/2}$	Station 119 SD	Average Stress Drop <SD>	ESD
Foreshocks											
1	0.5	.032	43	.035	33	.029	58			43	1.33
2	1.3	----	---	.030	137	.031	124			130	1.07
3	0.5	.035	33	.042	19	.014	511			68	5.85
4	0.6	.033	50	.024	129	----	---			80	1.97
5	0.5	.035	33	----	---	.031	47			39	1.29
6	3.4	.037	192	.033	270	.041	141			194	1.39
7	0.6	.021	193	.025	114	----	---			149	1.45
8	0.8	.063	11	.045	24	----	---			16	1.74
9	0.6	.050	14	.045	20	.046	18			17	1.18
Aftershocks											
1	2.7	----	---	.057	41	.059	37			39	1.08
2	7.0	.045	220	.043	252	.046	206			225	1.11
3	1.4	.033	108	.045	42	.026	220			100	2.29
4	3.6	.049	87	.055	61	.050	81			75	1.21
5	1.5	----	---	.029	179	.026	249			211	1.26
6	1.0	.024	210	.025	185	.025	185			193	1.08
7	1.2	.031	112	.026	191	.027	170			154	1.32
8	1.2	----	---	.019	500	.023	282			375	1.50
9	1.1	.047	30	.036	67	.036	67			51	1.59
10	5.2	----	---	.063	60	.056	85			71	1.28
11	1.1	.021	328	.023	250	----	---			286	1.21
12	2.5	.042	96	.044	83	.051	53			75	1.36
13	1.3	.031	124	.030	137	.026	210			153	1.32
14	2.7	.026	444	.025	500	----	---			471	1.09
15	1.5	.032	133	.024	316	.024	316			237	1.65
16	1.1	.038	57	.039	53	.032	95			66	1.37
17	3.6	.038	186	.039	172	.028	464			246	1.74
18	1.8	.042	68	.022	475	.035	118			156	2.72
19	1.7	.047	46	.062	20	.044	57			37	1.74
20	1.0	----	---	.043	36	.049	25			30	1.29
21	1.1	.041	44	.045	33	.040	48			41	1.22
22	1.9	----	---	.042	72	.046	54			62	1.23
23	1.7	.052	35	----	---	.044	58			45	1.43
24	2.1	.036	128	.028	273	.067	20			89	3.84

Table 3. (continued)

Source parameters of earthquakes listed in Table 2

Event* No.	Moment (10^{21} dyne-cm)	Station 104 $\zeta_{1/2}$	Station 104 SD	Station 112 $\zeta_{1/2}$	Station 112 SD	Station 115 $\zeta_{1/2}$	Station 115 SD	Station 119 $\zeta_{1/2}$	Station 119 SD	Average Stress Drop <SD>	ESD
25	1.0	.065	11	.056	16	----	---			13	1.30
26	2.1	----	---	.030	227	.031	206			216	1.07
27	2.1	.038	109	.038	109	.030	222			138	1.51
28	1.1	.026	182	.025	204	.036	68			136	1.83
29	1.6	.032	140	.032	140	.031	154			145	1.06
30	1.6	----	---	.026	255	.027	227			241	1.09
31	1.2	----	---	.029	144	.028	160			152	1.08
32	1.7	----	---	.037	95	.041	70			82	1.24
33	1.1	----	---	.026	182	.025	204			193	1.08
34	1.5	.030	162	.023	359	.023	359			275	1.58
35	1.5	.033	122	.042	59	.029	179			109	1.76
36	3.5	----	---	.033	277	.036	213			243	1.20
37	1.9	.039	92	----	---	.026	309			169	2.36
38	1.6	.030	166	.033	125	.033	125			137	1.18
39	1.9	.037	105	.037	105	.041	77			95	1.20
40	1.5	.052	30	.048	39	.045	47			38	1.25
41	2.9	.040	128	----	---	.033	228			171	1.50
42	1.3	.035	84	.043	45	----	---			61	1.55
43	3.0	----	---	.028	392	.036	184			269	1.71
44	1.3	.042	49	.038	66	.035	84			65	1.31
45	2.5	.027	369	.042	98	.141	3			48	12.01
46	1.2	.037	66	.031	112	.030	124			97	1.40
47	1.0	.025	185	.035	68	.036	62			92	1.83
48	4.8	.040	213	.038	248	.086	21			104	3.99
49	1.2	.040	55	.038	64	.033	98			70	1.35
50	1.6	.052	32	----	---	.051	34			33	1.04
51	1.4	.042	54	----	---	.031	133			85	1.89
52	1.4	.051	31	.045	45	----	---			37	1.30
53	1.4	.047	39	.038	74	----	---			54	1.57
54	3.8	.047	105	.049	93	.076	25	.092	14	43	2.69
55	1.1	.027	158	.028	142	.026	177	.033	87	136	1.37
56	3.0	.031	289	.030	319	----	---	.038	157	244	1.47
57	1.3	.055	22	.055	22	----	---	.063	15	19	1.25

@ for explanation of the symbols, see text.

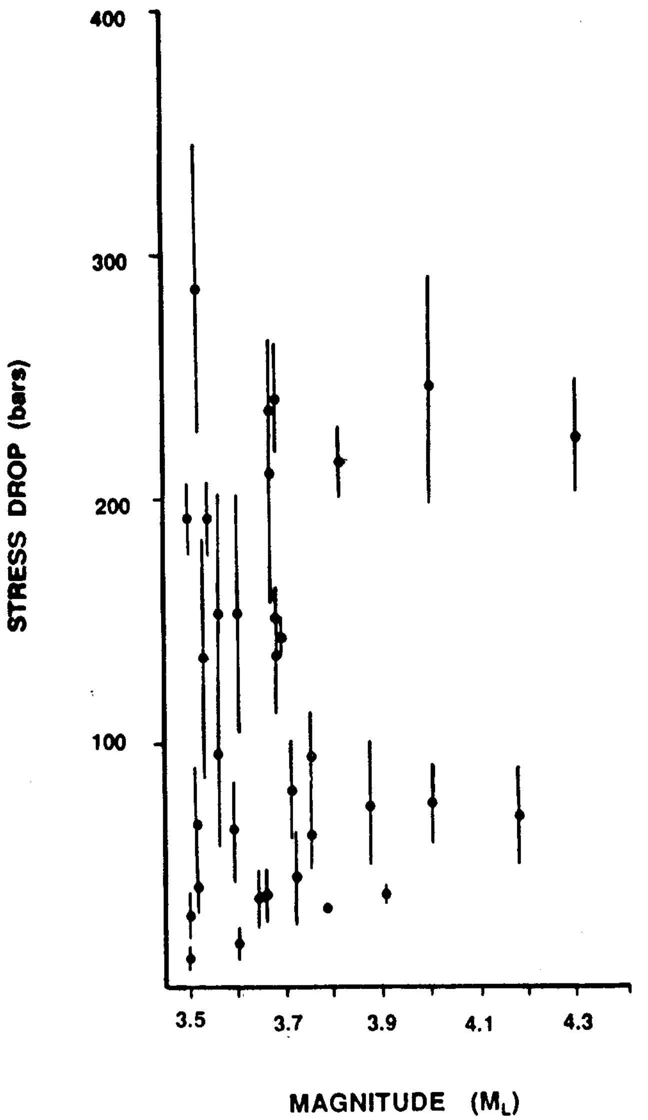

Fig. 3. Aftershock stress drop versus magnitude for events with ESD ≤ 1.45 (see Table 3). The bars indicate the estimated error.

be underestimated and the static stress drop overestimated. The average stress drops of Table 3, however, reduce the scatter inherent in the measurements and allow us to recover some gross properties of the source.

For the closest station (119) and the farthest station (112) to the center of the aftershock area, the same aftershock average minimum pulse width was observed (Table 1). We had expected the minimum pulse width difference to be largest between these two stations. Since station 119 shows the largest scatter in Figure 2 and is the only one located within the aftershock area proper (Figure 1), the pulse widths may have been strongly affected by the site response. This effect can broaden the pulse width of P-waves by as much as 0.08 s (Frankel and Kanamori, 1983). Thus the minimum pulse width (ζ_{min}) of these small events may be controlled partially by the propagation path, with an effect of the site response and/or the instrument response.

Figure 2 shows that different pulse widths occur for events of similar magnitude. This suggests that strong scattering effects or strong variations in intrinsic attenuation could be conditioning the signals. Since larger events ($M_L \geq 3.5$) are also affected by these two mechanisms, by subtracting the average minimum pulse width from the pulse width of the large events we are correcting for the effect of the path. The corrected pulse width can now be related to the rupture duration and hence to the stress drop. The effect of the source-receiver path on the initial pulse of the seismogram is essentially eliminated with this technique.

In Figure 2, the pulse width increases with magnitude but its minimum values remain almost constant up to magnitude 2.7 at least. This leveling off of pulse widths with magnitude was also reported by Frankel and Kanamori (1983) and O'Neill (1984), for earthquakes in California. It is interpreted as produced solely by propagation effects.

We noticed that in general the deeper events had simpler pulse shapes than the shallower ones. Apparently, the shallower events were located in areas which are structurally more complex and inhomogeneous.

Figure 4 shows the foreshock and aftershock stress-drop spatial distribution. For the foreshocks (Fig. 4f) we observe values ranging from 39 to 194 bars in the east part of the aftershock zone. The lower values (16 and 17 bars) are for events 8 and 9 (Table 3) located near the epicenter of the Petatlán earthquake. The corrected $\zeta_{1/2}$ value (Table 3) for these events is significantly larger than for the other events (1 to 7) at all stations. This suggests that the rupture duration of events 8 and 9 was larger than for the other events. Since we assumed the same rupture velocity for all earthquakes, the fault radius for these two events was large and their stress drop must have been low, as was in fact observed.

The area surrounding the focus of an impending earthquake is expected to be under high stress. Pechmann and Kanamori (1982) reported a larger stress drop for foreshocks near the maximum surface displacement in the 1979 Imperial Valley earthquake. Earthquakes are assumed to result when the stress buildup eventually exceeds some critical local strength. If the stress drops correlate with the state of stress in the region, our results suggest that the western part of the aftershock zone (where the mainshock occurred) had a lower stress level than the eastern part. With only two events near the mainshock this observation is not conclusive. However, Novelo-Casanova *et al.* (1984) and Hsu *et al.* (1985), concluded that two asperities were broken in the rupture plane. They based their results on seismic patterns, spatial distribution of local seismic activ-

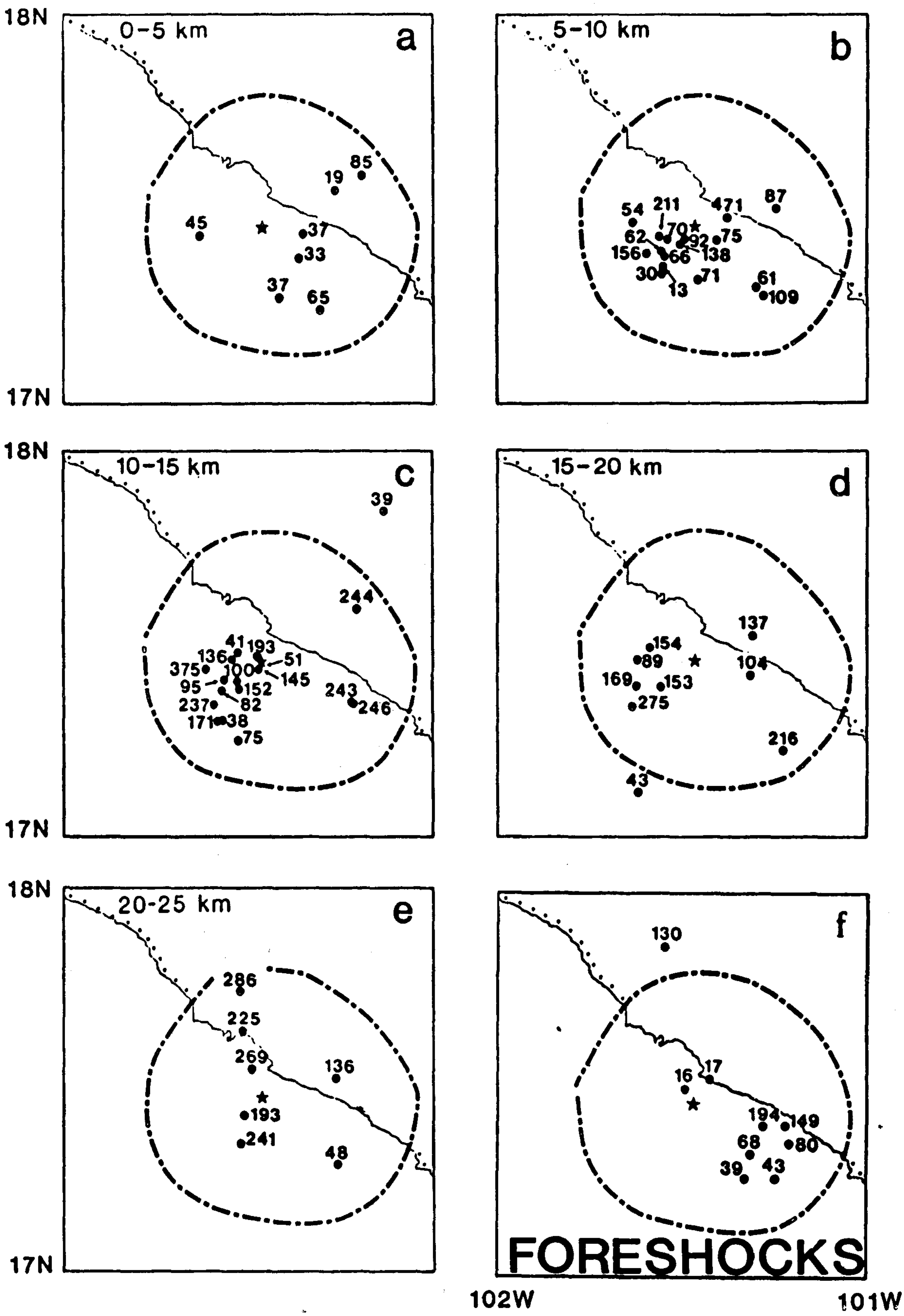

Fig. 4. (a to e) Average aftershock stress drops at different depth intervals. (f) Foreshock stress-drop distribution; the depths of foreshocks range from about 1.5 km to 14.0 km (Table 2).

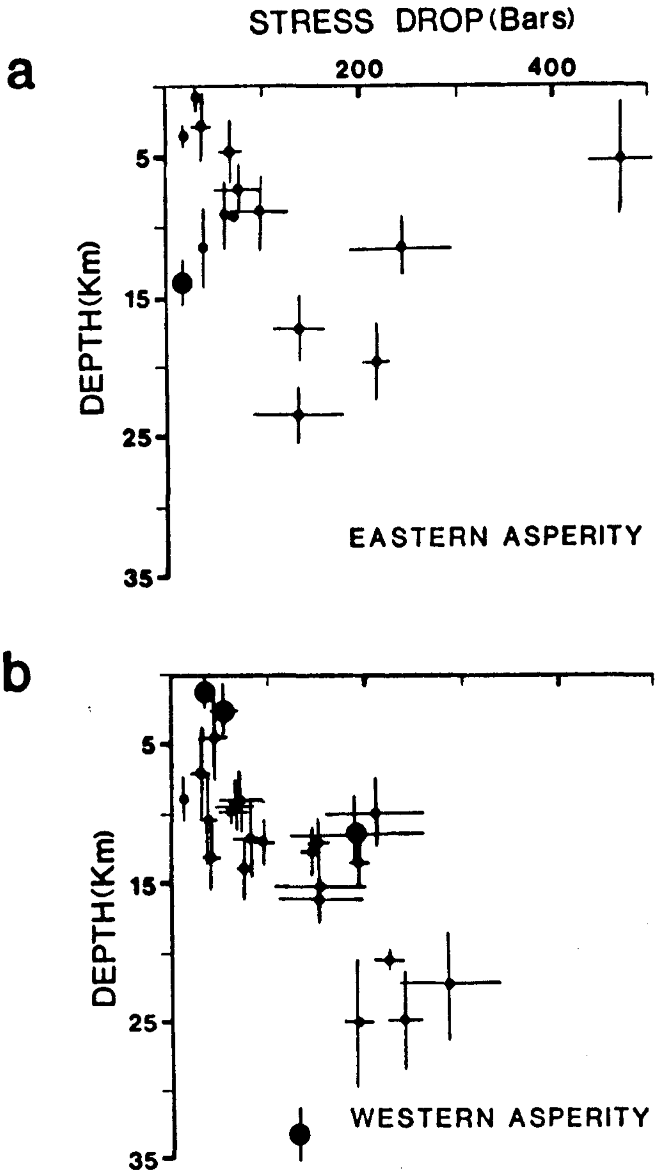

Fig. 5. Foreshocks (large circles) and aftershocks (small circles). Stress drops versus depth for the eastern (a) and western (b) asperities for events with ESD ≤ 1.45 (see Table 3). The bars indicate the estimated error.

ity, and energy release before and after the Petatlán earthquake. The present results suggest that the eastern asperity was releasing stress while the western one was accumulating stress before the mainshock.

The average aftershock stress drop shows an irregular stress distribution throughout the aftershock area (Fig. 4 a - e). The zones of relative high and low stress drops are not clearly defined. There are some indications, however, that maximum values of stress drop increase with depth.

Depth-dependence of the stress drop is not generally observed everywhere. Frankel and Kanamori (1983) and O'Neill (1984) did not find any stress-drop-depth dependence for earthquakes in California. Fletcher *et al.* (1983), however, observed a static stress drop strongly dependent on depth for microearthquakes with focal depths between 0.07 and 1.40 km. In the aftershocks of the Oroville earthquake, largest stress drops occurred for the deepest events and no large stress drops occurred at shallow depths (Fletcher *et al.*, 1984).

The foreshock and aftershock stress-drop-versus-depth distribution was analyzed in each of the two presumed asperities. Figure 5 shows that the stress-drop envelope for the western asperity increases with depth marginally faster than for the eastern asperity.

This result implies that for a given depth, the stress drops were higher in the western than in the eastern asperity. Yet foreshock stress drops were higher in the eastern region, as we just indicated. This too suggests two zones with different stress and strength concentration, though the result is not conclusive because of possible errors in depth determinations.

It is important to note that the details of the rupture process were obtained entirely from pre- and post-seismic activity as recorded by a local array. Such details of the source rupture are not found on teleseismic long-period records (Chael and Stewart, 1982; Singh *et al.*, 1984).

CONCLUSIONS

The method proposed here has limitations involving the instrumentation and the variability of the data. One question is whether the waveforms of the events used as Green's functions accurately reflect the minimum value of pulse width for a particular station. Errors in estimating the minimum $\zeta_{1/2}$ can also be important in the stress drop estimation. By averaging results from several stations for each event, this problem can be controlled.

Another question is raised by the dependence of the stress drop on rupture velocity. A constant rupture velocity equal to 3.75 km/s was used for all events. The actual rupture velocities may vary from one event to another. Thus, some of the differences in stress drops may actually be caused by different rupture velocities.

This study suggests that the foreshock and aftershock stress drops of the Petatlán earthquake support a two-asperity model in the source area as proposed by Novelo-Casanova *et al.* (1984) and Hsu *et al.* (1985). Before the mainshock, the eastern asperity was releasing stress while the western one was accumulating it. When the western asperity was unable to withstand the tectonic stress load and the failure took effect, the Petatlán earthquake occurred.

Aftershock stress drops were irregularly distributed throughout the aftershock area, indicating a pronounced heterogeneity in the source region after the main shock had occurred.

ACKNOWLEDGEMENTS

I am grateful to Eduard Berg and Charles E. Helsley for helpful discussions during this study. I thank two anonymous reviewers for their valuable suggestions. I also wish to thank Patricia Medina for her assistance in typing the manuscript.

BIBLIOGRAPHY

ARCHULETA, R. J., E. CRANSWICK, C. MUELLER and P. SPUDICH, 1982. Source parameters of the 1980 Mammoth Lakes, California, earthquake sequence. *J. Geophys. Res., 87,* 4595-4608.

BOATWRIGHT, J., 1980. A spectral theory for circular seismic sources: simple estimates of source dimensions, dynamic stress drop, and radiated seismic energy. *Bull. Seism. Soc. Am., 70,* 1-27.

BRUNE, J. N., 1970. Tectonic stress and the spectra of seismic shear waves from earthquakes. *J. Geophys. Res., 75,* 4997-5009.

CHAEL, E. P. and G. S. STEWART, 1982. Recent large earthquakes long the Middle America Trench and their implication for the subduction process. *J. Geophys. Res., 87,* 329-338.

EWING, J. and R. P. MEYER, 1982. Rivera Ocean Seismic Experiment (ROSE) overview. *J. Geophys. Res., 87,* 8345-8357.

FLETCHER, J. B., J. BOATWRIGHT and W. B. JOYNER, 1983. Depth dependence of source parameters at Monticello, South Carolina. *Bull. Seism. Soc. Am., 73,* 1735-1751.

FLETCHER, J. , J. BOATWRIGHT, L. HAAR, T. HANKS and A. McGARR, 1984. Source parameters of aftershocks of the Oroville, California earthquake. *Bull Seism. Soc. Am., 74,* 1101-1123.

FRANKEL, A. and H. KANAMORI, 1983. Determination of rupture duration and stress drop for earthquakes in southern California. *Bull. Seism. Soc. Am., 73,* 1527-1551.

GETTRUST, F. J., V. HSU, C. E. HELSLEY, E. HERRERO and T. JORDAN, 1981. Patterns of local seismicity preceding the Petatlán earthquake of March 14, 1979. *Bull. Seism. Soc. Am., 70,* 761-769.

HSU, V., J. F. GERTTRUST, C. E. HELSLEY and E. BERG, 1983. Local seismicity preceding the March 14, 1979, Petatlán, Mexico earthquake (M_s = 7.6). *J. Geophys. Res. 88,* 4247-4262.

HSU, V., C. E. HELSLEY, E. BERG and D. A. NOVELO-CASANOVA, 1985. Correlation of foreshocks and aftershocks and asperities. *Pure App. Geophys., 122,* 878-893.

NOVELO-CASANOVA, D. A., V. HSU, E. BERG, C. E. HELSLEY and J. F. GETTRUST, 1984. Aftershock activity of the Petatlán earthquake: The first 54 hours. *Bull. Seism. Soc. Am., 74,* 2451-2461.

O'NEILL, M. E., 1984. Source dimensions and stress drops of small earthquakes near Parkfield, California. *Bull. Seism. Soc. Am., 74,* 27-40.

PECHMANN, J. C. and H. KANAMORI, 1982. Waveforms and spectra of preshocks and aftershocks of the 1979 Imperial Valley, California, earthquake: Evidence for fault heterogeneity. *J. Geophys. Res., 87,* 10579-10597.

SINGH, S. K., T. DOMINGUEZ, R. CASTRO and M. RODRIGUEZ, 1984. P waveform of large, shallow earthquakes along the Mexican subduction zone. *Bull. Seism. Soc. Am., 74,* 2135-2156.

D. A. Novelo-Casanova
Instituto de Geofísica, UNAM,
04510 - México, D. F., México.